ACS OMEGA

http://pubs.acs.org/journal/acsodf

Article

Nonbenzenoid BODIPY Analogues: Synthesis, Structural Organization, Photophysical Studies, and Cell Internalization of Biocompatible *N-Alkyl*-Aminotroponyl Difluoroboron (*Alkyl*-ATB) Complexes

Bibhuti Bhusana Palai, Supriya Kumari, Manjusha Dixit, and Nagendra K. Sharma*

Cite This: *ACS Omega* 2022, 7, 27347−27358

Read Online

ACCESS | Metrics & More | Article Recommendations | Supporting Information

ABSTRACT: The *alkyl*-BODIPY derivatives are lipid types of fluorescent molecules that exhibit a unique structure and functions including sensing of hydrophobic microenvironments in living cells. Their synthesis involves multisteps from the core structure dipyrromethene scaffold. The *alkyl*-BODIPY analogues are sought to derivatize with minimal synthetic steps even by altering the core structures derived from benzenoid aromatic moiety. Recently, the nonbenzenoid scaffold (aminotropone) has been explored to synthesize troponyl-BODIPY analogues, which are fluorescent. In the repertoire of nonbenzenoid analogue, *N-alkyl*-aminotroponyl difluoroboron (*alkyl*-ATB) is rationally designed comprising long-chain hydrocarbons to explore the lipid type of fluorescent molecules. This report describes the synthesis, photophysical studies, structural organization, and biocompatibilities of ATB derivatives containing different lengths of alkyl chain at 2-aminotropone scaffold. The photophysical studies of ATB derivatives reveal their fluorescence behaviors in organic solvents (CH_3OH/CH_3CN) with a quantum yield of ∼10 to 15%. These ATB derivatives also exhibit fluorescence characters in the solid state though their quantum yield is relatively low. Cell permeability and cytotoxicity studies reveal that *alkyl*-ATB derivatives are permeable to HeLa/HEK293T cell lines and show negligible cytotoxicity. The biocompatibility of *alkyl*-ATB derivatives is studied and confirmed by cell viability (MTT) assay to the HeLa/HEK293T cell lines. Importantly, the cell internalization studies of the representative *alkyl*-ATB molecule by fluorescence microscopy show that *octyl*-ATB is efficiently detectable at the cytoplasmic membrane and cellular nucleus in HeLa cells. Hence, *alkyl*-ATB derivatives are potential fluorescent molecules for developing probes to visualize cellular components under a fluorescence microscope.

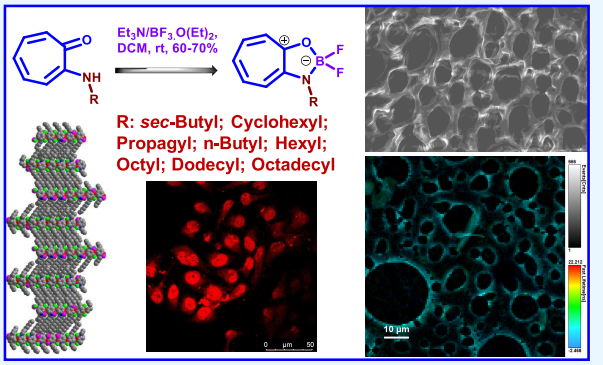

INTRODUCTION

Boron-dipyrromethene (BODIPY) derivatives are versatile synthetic fluorescent molecules for labeling biomolecules and synthesis of energy-related cassette entities (Figure 1A).[1−4] However, the unsubstituted BODIPY molecule is chemically less stable and nonfluorescent. Thus, various substituted dipyrromethene scaffolds are synthesized for tuning the structural and functional properties, including solubility, and dye properties.[5,6] For example, *alkenyl*-BODIPY exhibits absorption peaks in the near-infrared region (NIR);[7] dipyridylmethene (DIPYR) dyes[8] pyridine-based BODIPY analogues exhibit a wide range of photophysical properties, from nonemissive to green fluorescence with quantum yield 0.2−0.8;[9] BOIMPYs, benzimidazole-containing analogue, show red-emissive fluorophores, considered as NIR dyes.[10] Werz synthesized super-fluorophores comprising ethylene-bridged oligo-BODIPYS with quantum yield almost unity.[11] Recently, a new class of BODIPY dyes as *N*-BODIPYs (diaminoboron dipyrromethanes) are prepared for developing photonic materials.[12] In the literature, it is reported that BODIPY derivatives comprising longer linear alkyl chains can minimize their molecular aggregation problem owing to the $\pi-\pi$ stacking and are capable of forming self-assembled supramolecular structures.[13] For example, long-alkyl-chain-containing fluorescence peptides have been applied as a probe for the fluidity changes in cell membranes or sol-to-gel transition.[9,14,15] Importantly, the lipophilic BODIPY analogues are used as fluorescence probes for the lipid environment.[16] However, the synthesis of lipid-BODIPY analogues involves multistep synthesis from nondipyrromethene scaffolds. Thus, nondipyrromethene scaffolds are sought to prepare BODIPY

Received: April 16, 2022
Accepted: July 19, 2022
Published: August 1, 2022

https://doi.org/10.1021/acsomega.2c02379
ACS Omega 2022, 7, 27347−27358

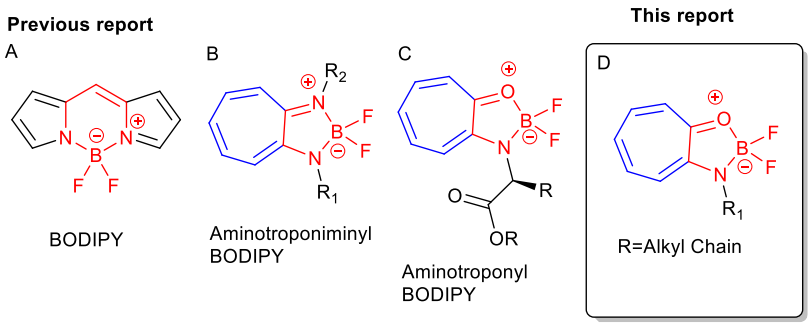

Figure 1. Chemical structures previously reported and new compounds: (A) BODIPY; (B) aminotroponimine difluoroboron; (C) aminoacidyltropone difluoroboron; and (D) alkyl-aminotroponyl difluoroboron (this work).

Scheme 1. Synthesis of *Alkyl*-Aminotroponyl Difluoroboron Complexes

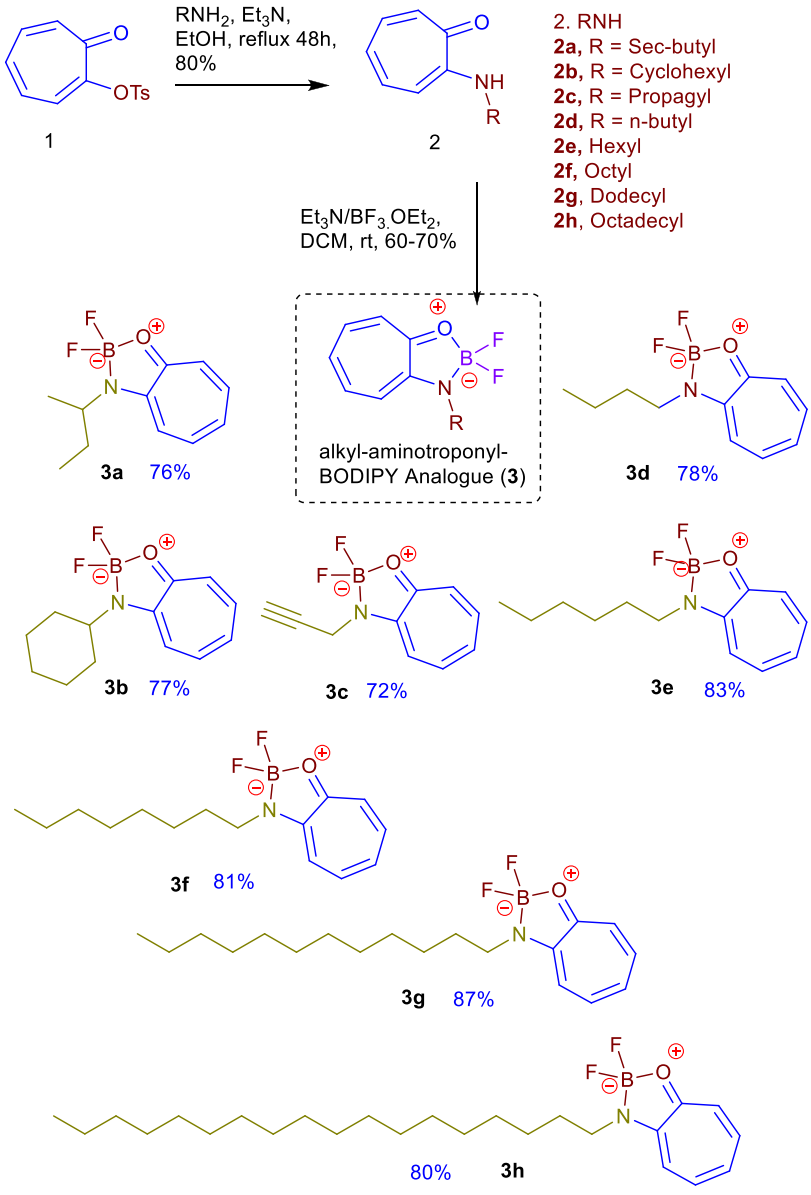

analogues from the benzenoid aromatic core structures that could be synthesized easily and elegantly. However, non-benzenoid aromatic core structures are also known and are constituents of various natural products. These ligands are derived from tropolone. This nonbenzenoid aromatic molecule is a constituent of troponoid natural products, such as colchicine, thujaplicine, manicoline, theaflavin, and isoimerubrin.[17−19] Its related derivatives show unusual photophysical behavior owing to the $\pi-\pi^*$, $n-\pi^*$, and intramolecular charge transfer.[20−22] The fluorescence behavior of tropolone is

https://doi.org/10.1021/acsomega.2c02379
ACS Omega 2022, 7, 27347−27358

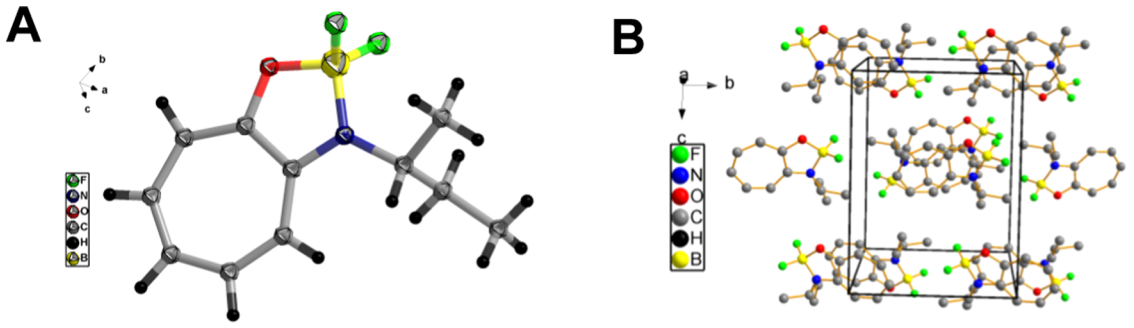

Figure 2. X-ray analysis of *propargyl*-ATB (**3a**): ORTEP diagram (A); unit cell packing diagram (B).

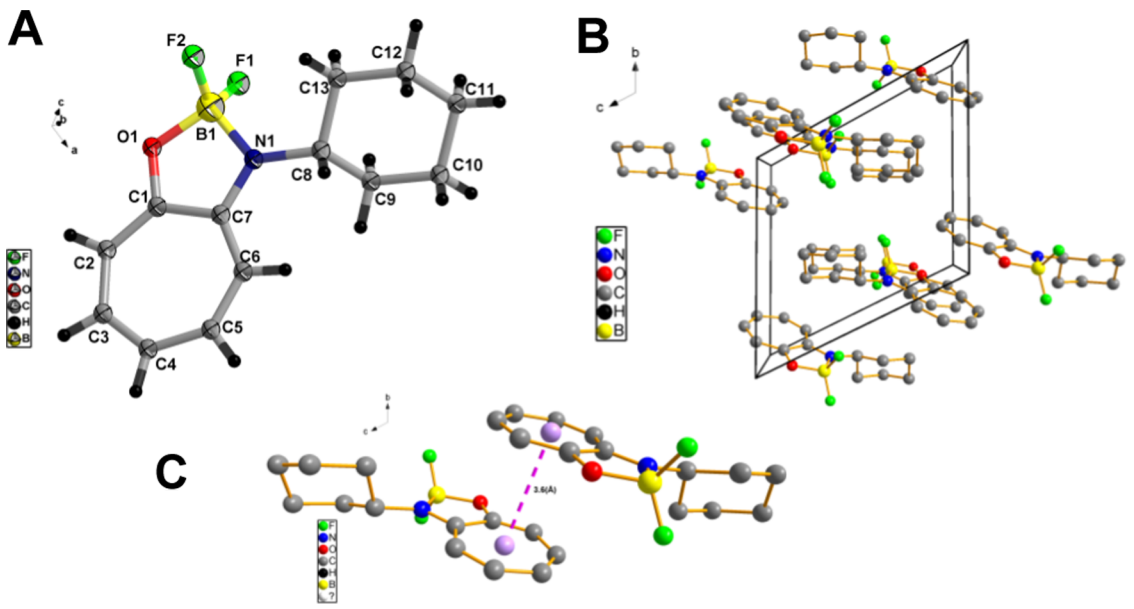

Figure 3. X-ray analysis of *cyclohexyl*-ATB (**3b**): ORTEP diagram (A) and unit cell packing diagram (B); $\pi-\pi$ interaction between troponyl ring (C).

sensitive to environments' polarity and pH conditions, although its fluorescence quantum is low.[23,24] Tropolone and its synthetic derivatives are ligands of two various coordinating metal ions. Previously, we have explored nonbenzenoid aromatic scaffolds such as 2-aminotropones and 2-aminotropimines for the synthesis of BODIPY analogues from aminotropone derivatives via *N,N*-/*N,O*-chelation (Figure 1B,C).[25,26] These analogues exhibit fluorescence properties with a quantum yield of ca. ∼0 to 15%. However, *N,O*-chelated *troponyl*-BODIPY analogues comprise various amino acid carboxylate functionalities (Figure 1C).[26] In the literature, lipophilic BODIPY analogues are synthesized by conjugating the long-chain alkyl group at the BODIPY core structure for sensing cellular hydrophobic environments.[27,28] In the repertoire of lipophilic BODIPY analogues, we rationally designed *alkyl*-aminotroponyl difluoroboron complex containing different lengths of hydrocarbon chain (Figure 1D). This report describes their synthesis, structural analysis, and photophysical properties. This report also demonstrates their self-assembly structural morphologies and fluorescence properties in the solid-state surface. Herein, their biocompatibility is also explored in vivo with HeLa/HEK-292 cell lines.

RESULTS AND DISCUSSION

We began the synthesis of boron-aminotropone complexes from commercially available tropolone (Scheme 1). Tropolone was converted to 2-tosyltropone (**1**) by following the previous method.[26] This tosylate derivative (**1**) was treated with various *alkyl*-amine under reflux conditions, producing *N*-substituted aminotropones derivatives (**2**). We used *isobutyl*-amine, *butyl*-amine, *cyclohexyl*-amine, *propargyl*-amine, *hexyl*-amine, *octyl*-amine, *dodecyl*-amine, and *octadecyl*-amine for the synthesis of respective *N*-alkyl-aminotropone ligands (**2a−2h**). These ligands (**2a−2h**) were purified by silica gel column chromatography and characterized by $^{1}H/^{13}C$ NMR and ESI-HRMS. Their characterization data are provided in the Supporting Information (Figures S1−S16). These *alkyl*-aminotropone ligands were treated with versatile difluoroboronating reagent $BF_3.OEt_2$ under the mild basic condition produced rationally designed *alkyl*-aminotropony-BODIPY (*alkyl*-ATB) analogues (**3a−3h**). We isolated *isobutyl*-ATB (**3a**), *cyclohexyl*-ATB (**3b**), *propargyl*-ATB (**3c**), *butyl*-ATB (**3d**), *hexyl*-ATB (**3e**), *octyl*-ATB (**3f**), *dodecyl*-ATB (**3g**), and *octadecyl*-ATB (**3h**). These complexes (**3a−3h**) were purified by silica gel column chromatography using ethylacetate/hexane (10:90) and isolated in good yields (80%), and were characterized by NMR (^{1}H, ^{13}C, ^{11}B, ^{19}F NMR) and ESI-

https://doi.org/10.1021/acsomega.2c02379
ACS Omega 2022, 7, 27347−27358

HRMS. Their data are provided in the Supporting Information (Figures S17−S45).

We attempted to crystallize *alkyl*-ATB derivatives in organic solvent systems for structural studies. Pleasantly, we obtained single crystals of four derivatives (**3a**/**3b**/**3c**/**3g**) in the DCM/MeOH solvent system and studied them using a single-crystal diffractometer. Their solved X-ray data were deposited at the Cambridge Crystallographic Data Centre (CCDC) with reference numbers 2158349 for **3a**, 2158348 for **3b**; 2158346 for **3c**; and 2158347 for **3d**. Their ORTEP and unit cell packing diagrams are provided in Figures 2 and 3, while their other crystal structure parameters are tabulated in the Supporting Information (Figures S46−S49 and Tables S1−S4). The ORTEP diagram of *isobutyl*-ATB (**3a**) shows the chemical structure. In contrast, the unit cell packing diagram shows the presence of more than two molecules in the unit cell through the noncovalent interaction, mainly through intermolecular hydrogen bonding as F···H−C (Figure 2A,B). The selected bond length and bond angles are given in Table 1.

Table 1. Selected Bond Lengths and Bond Angles of Boron Complexes 3a in the Solid State

selected bond lengths	selected bond angles	selected bond angles
C1−C7 = 1.446 Å	O1−B1−N1 = 99.31°	B1−O1−C1 = 99.31°
C1−O1 = 1.313 Å	F1−B1−O1 = 109.92°	B1−N1−C7 = 110.68°
C7−N1 = 1.329 Å	F2−B1−N1 = 112.34°	O1−C1−C7 = 110.55°
O1−B1 = 1.487 Å	F1−B1−N1 = 113.67°	N1−C7−C1 = 107.79°
N1−B1 = 1.548 Å	F2−B1−O1 = 111.02°	F1−B1−F2 = 110.13°

Their lengths and bond angles are within the range. Generally, lipids form a bipolar self-assembly supramolecular structure by the interaction of head−head/tail−tail residue.[29,30] The packing arrangement of crystal **3a** shows the orientation of troponyl difluoroboron residue (polar group, equivalent to the head of the lipid) and *isobutyl* residue (nonpolar group, comparable to the tail of lipid), which are nonplanar and do not exhibit lipid type of head−head/tail−tail residual interactions in the packing arrangement of crystal **3a**.

The OTEP diagram *cyclohexane*-ATB (**3b**) shows its chemical structure. In contrast, the unit cell packing diagram shows the presence of more than two molecules in the unit cell through a unique noncovalent $\pi-\pi$ interaction between *troponyl* rings with a bond distance of 3.6 Å along with intermolecular hydrogen bonding as F···H−C (Figure 3A−C). In the packing arrangement of crystal **3b**, the orientations of troponyl difluoroboron residue (polar group, equivalent to the head of the lipid) and *cyclohexyl* residue (nonpolar group, comparable to the tail of lipid) are almost in the same plane as a lipid type of head−head interaction.

The ORTEP diagram of *propargyl*-ATB (**3c**) shows its chemical structure. In contrast, the unit cell packing diagram exhibits the presence of more than one molecule through the noncovalent π-π interactions between troponyl rings with a bond distance of 3.7 Å (Figure 4A−C). Similarly, an intermolecular hydrogen bonding as F···H−C also occurs in packing arrangement. In the packing structure of crystal **3c**, the orientations of troponyl difluoroboron residue (polar group, equivalent to the head of the lipid) and propargyl residue (nonpolar group, comparable to the tail of lipid) are almost in the opposite plane but exhibit a lipid type of head−head interaction.

The ORTEP and packing diagrams of *dodecyl*-ATB (**3g**) are provided in Figure 5A−E. The crystal structure of *dodecyl*-ATB (**3g**) shows a unique bipolar arrangement in its unit cell (Figure 5B). Noncovalent $\pi-\pi$ interactions are found between their troponyl ring with a distance of 3.7 Å, and hydrophobic interactions are found between lipophilic *dodecyl* residues (Figure 5C). The space-filled model shows the formation of sheet-type 3D structures (Figure 5D). Its long-chain and difluoroboron residues are oriented at ∼120°, unlike other ATB crystals **3a**−**3c** (Figure 5E). This rearrangement strongly supports the formation of three-dimensional lipid-type structure through head−head and tail−tail interactions.

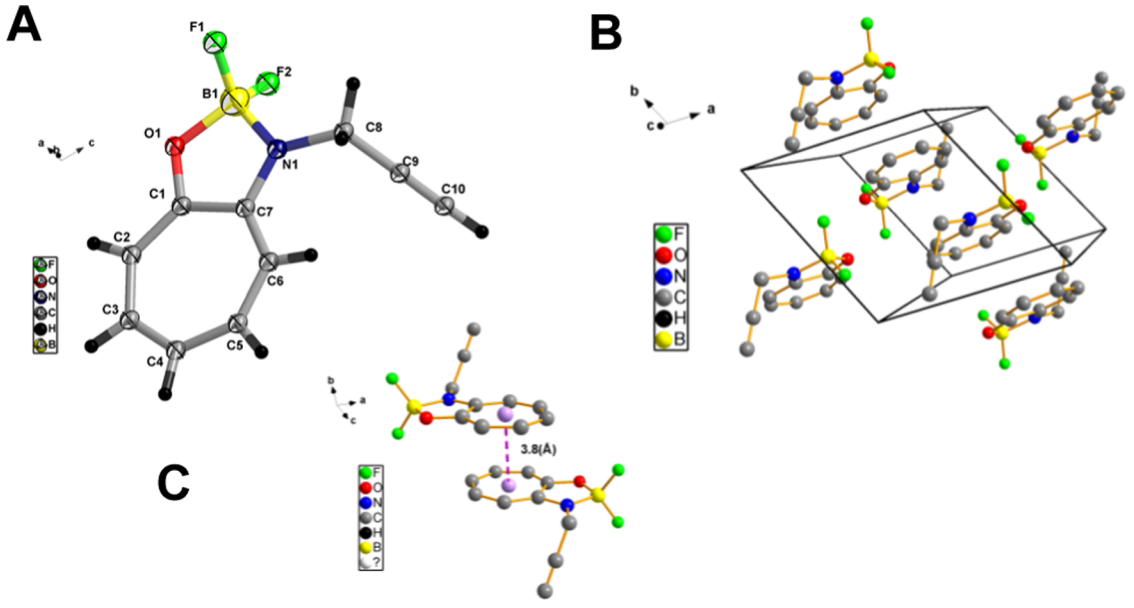

Figure 4. X-ray analysis of *propargyl*-ATB (**3c**): ORTEP diagram (A); unit cell packing diagram *propargyl*-ATB derivative (B) and $\pi-\pi$ interaction between troponyl rings (C).

https://doi.org/10.1021/acsomega.2c02379
ACS Omega 2022, 7, 27347−27358

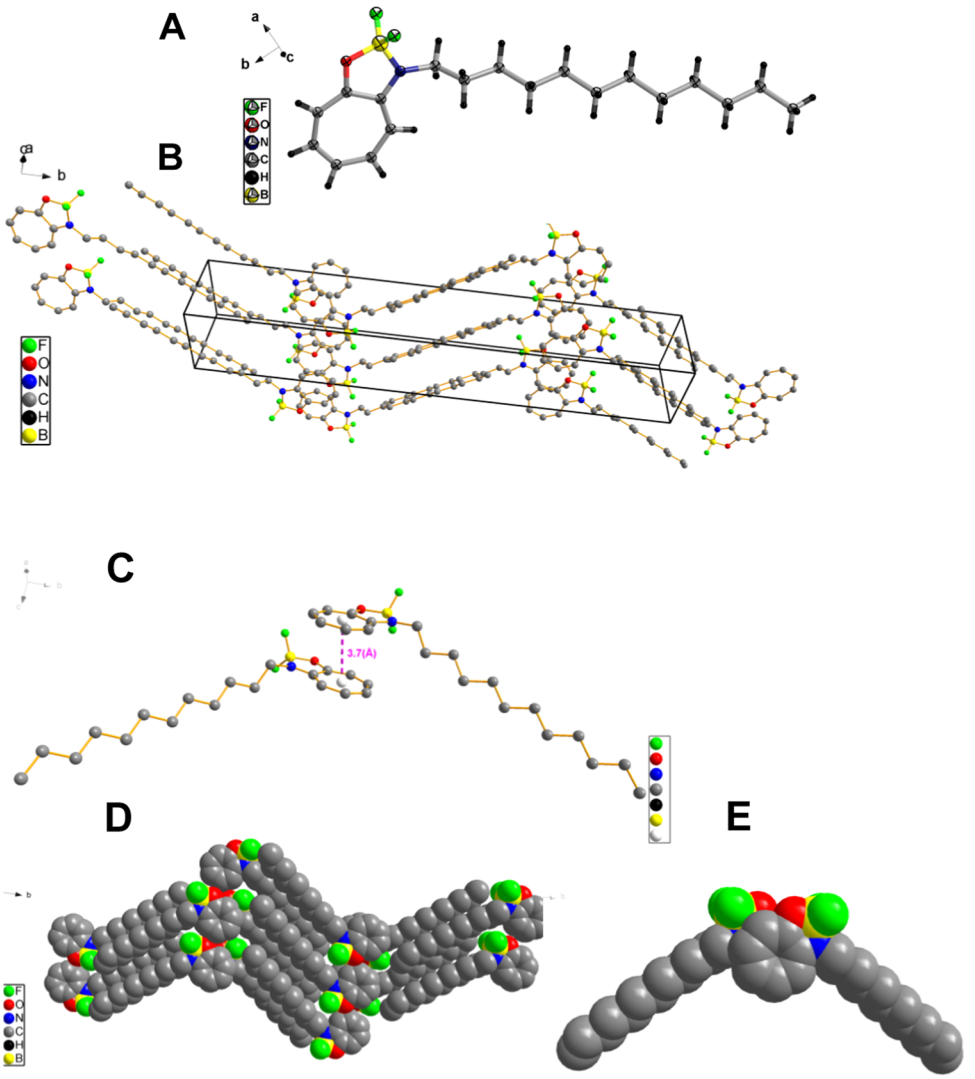

Figure 5. X-ray analysis of *octadodecyl*-ATB (**3g**): ORTEP diagram (A); unit cell packing diagram (B); $\pi-\pi$ interaction between troponyl ring (C); space-filled model of unit cell (D); and $\pi-\pi$ interaction in space-filled model (E).

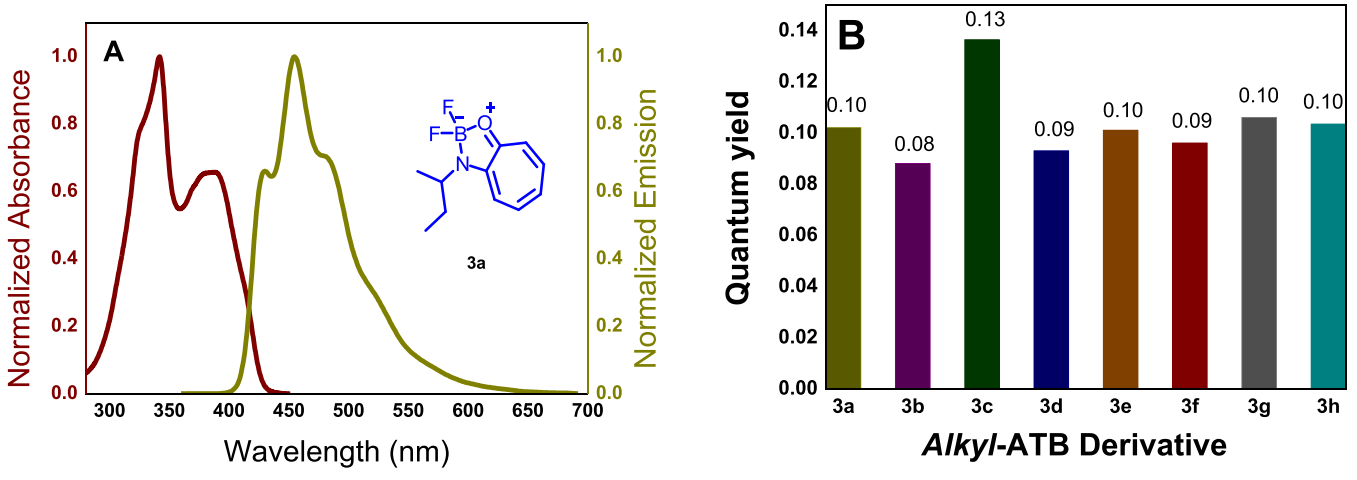

Figure 6. (A) Normalized absorption and emission spectra of *isobutyl*-ATB derivative (**3a**) in MeOH at the concentration (5×10^{-4} M); for other derivatives, see the Supporting Information. (B) Bar diagram of quantum yield of *alkyl*-ATB derivatives (**3a**–**3h**) insolvent MeOH.

Photophysical Studies. We recorded the absorption and emission spectra of newly synthesized *N-alkyl*-aminotroponyl-BODIPY lipid analogues (**3a**–**3h**) in organic solvent methanol (MeOH)/acetonitrile (ACN). Their full-range UV–vis/fluorescence spectra are provided in the Supporting Information (Figures S50 and S51). The normalized

https://doi.org/10.1021/acsomega.2c02379
ACS Omega 2022, 7, 27347−27358

absorbance and fluorescence spectra of *isobutyl*-ATB complex (**3a**) in MeOH are depicted in Figure 6A. However, the normalized absorbance and emission spectra of *alkyl*-ATB (**3a−3h**) in both solvent MeOH/ACN are also provided the Supporting Information for finding the Strokes shift (Figures S53 and S54). We also extracted and calculated their photophysical parameters in both solvents (MeOH/ACN), which are summarized in the Supporting Information (Tables S5 and S6). Their absorption spectra exhibit three peaks at wavelengths (λ) ∼245, ∼340, and ∼390 nm in both solvents, mainly due to the $\pi-\pi^*$, n$-\pi^*$, and charge transfer transition in the aminotropone-difluoroboron residue. We also determined their extinction coefficients (ε) at $\lambda_{390\,nm}$ in MeOH (Table S5, column 5). The octadecyl aminotroponyl difluoroboron complex (**3h**) has a lower ε value (∼5.8 × 10^3 M^- cm^{-1}) compared to other analogues (∼9.0 × 10^3 M^{-1} cm^{-1}). Their emission spectra exhibit an intense peak at wavelength 455 nm ($\lambda_{em,455\,nm}$) and excitation wavelength 340 nm ($\lambda_{ex,340\,nm}$) with Stock's shift ca. ∼110 nm in MeOH. Thus these analogues are fluorescent, almost like our previously reported amino acid comprising BODIPY analogues.[26] We measured their (**3a−3h**) relative quantum yield (Φ_f) in MeOH/ACN at a temperature of 20 °C compared to reference standard 0.1 M quinine sulfate in H_2SO_4. Their values are provided in the Supporting Information (Tables S5−S8). We plotted a bar diagram of the quantum yield of **3a−3h** vs *alkyl*-ATB in MeOH (Figure 6B). Their quantum yields are ca. 9−13% (Tables S5 and S6, column 8). However, the quantum yield of *propargyl*-ATB (**3c**) is slightly higher (by ∼3%) compared to other analogues (**3a/3b/3d−3h**) in MeOH, possibly owing to the π-electron-rich alkyne group, which may lower the HOMO−LUMO energy gap. The quantum yield of *alkyl*-ATB derivatives is less variable compared to the previously reported amino acidyl-troponyl difluoroboron complexes (Figure 1C).[26] The quantum yields of those amino acid fluorescent derivatives significantly varied with the bulkiness nature of substituents at α-C, such as glycine derivatives, which exhibit ∼15% while phenylalanine derivatives exhibit ∼6%. Their quantum yields have significantly dropped with branching α-C of amino acid residue and increasing carbon chain at the aminotropone ring. Herein, we also note that the quantum yield of cyclohexyl-substituted ATB derivative (**6b**) is decreased significantly with branching α-C compared to the alkynyl-substituted one (**3c**), while there are no significant changes with increasing carbon chain length. We also recorded the solvent-dependent quantum yield of long-chain *octadecyl*-ATB (**3h**) derivative (most lipophilic analogue) in nonpolar solvent systems such as DCM and cyclohexane, and chloroform. Their quantum yields and other photophysical parameters are provided in Table 2. Importantly, the quantum yield of **3h** has slightly increased compared to protic solvent MeOH. We plotted a bar diagram of the quantum yield of **3h** vs solvent (Figure 6B). We noted that the quantum yield of **3h** is reasonably high in the nonpolar solvent cyclohexane, possibly due to the strong lipophilic interaction, which could provide more rigidity in its structure. Thus, *alkyl-ATB* derivatives have some sort of fluorescence selectivity in a nonpolar solvent. We also recorded the fluorescence spectra of long-chain *alkyl*-ATB (**3f,3g/3h**) derivatives in a solid state at two different excitation wavelengths (340/380 nm). Their emission spectra are provided in the Supporting Information (Figure S55). We noted that *octyl*-ATB (**3f**) exhibits better fluorescence with an emission peak at wavelength 430 nm compared to the *dodecyl*-ATB (**3g**) and *octadecyl*-ATB (**3h**) at excitation wavelengths 340 nm. However, *octyl*-ATB (**3f**) and *dodecyl*-ATB (**3g**) exhibit almost the same fluorescence with an emission peak at wavelength 430 nm and excitation wavelength 380 nm. To examine the photostability of *alkyl*-ATB derivatives, we irradiated three representative compounds (**3d/3f/3g**) with UV light ($\lambda_{254\,nm}$, Hand UV-Lamp) at different time intervals and sequentially recorded UV−vis spectra (Figure S56). Their UV absorbance significantly decreased wavelength (λ) 250 nm with time compared to $\lambda_{350-400\,nm}$ with two isosbestic points $\lambda_{266\,nm}$ and $\lambda_{400\,nm}$ along with marginal redshift. These studies support the degradation of *alkyl*-ATB derivative with light. Hence, these alkyl-ATB derivatives are potential fluorescent analogues for applying in new fluorescence probe designs.

Table 2. Quantum Yields of Octadecyl-ATB (3h)[a]

solvents	λ_{abs} (nm)	abs	λ_{em} (nm)	Stoke's shift (nm)	OD/abs (nm)	Φ_f
methanol	334, 380	0.06085	417, 438	104	334	0.10
acetonitrile	335, 380	0.07202	415, 441	106	340	0.10
DCM	335, 382	0.08749	416, 443	108	346	0.12
cyclohexane	337, 385	0.08650	418, 442	105	345	0.13
chloroform	343, 394	0.06974	431, 556	113	346	0.13

[a]All measurements and quantum yields were determined for boron complex (**3h**) by considering quinine sulfate in 0.1 M H_2SO_4 as the standard reference.

The lipid molecules are prone to form liposome and micelles types of self-assembly supramolecular structures.[31] The packing diagram of the *alkyl*-ATB derivative's crystal reveals the formation of a self-assembly structure in the solid state through noncovalent interactions such as C−H···F hydrogen bonding, $\pi-\pi$ interactions, and hydrophobic interactions. In ethanol, we dissolved *alkyl*-ATB derivatives (**3b/3e/3f/3g/3h**). We prepared their respective thin-layer surfaces at silicon wafers for studying surface morphologies with field emission scanning electron microscopy (FE-SEM). The SEM images of *alkyl*-ATB (**3e−3h**) at the 10 uM scale are provided in Figure 7, while that of *cyclohexyl*-ATB (**3b**) is provided in the Supporting Information (Figure S56); their SEM images at other scales are provided in the Supporting Information (Figures S56−S60). The SEM images of *cyclohexyl*-ATB (**3b**) show the formation of crystalline structure, possibly owing to the $\pi-\pi$ interactions between head groups as troponyl ring (Figure S57). However, the SEM images of *hexyl*-ATB (**3e**), *octyl*-ATB (**3f**), *dodecyl*-ATB (**3g**), and *octadecyl*-ATB (**3h**) are significantly different from *cyclohexyl*-ATB (**3b**). The *hexyl*-ATB derivative (**3e**) forms a ring-type structure at the surface (Figure 7A). The *octyl*-ATB with lipophilic interaction and head−tail-type orientation. The *octanyl*-ATB (**3e**) forms a honey-comb type of surface morphology (Figure 7B). The *dodecyl*-ATB (**3g**) shows the flower-type surface structure, possibly due to the head−tail type of lipid structure (Figure 7C). The *octadecyl*-ATB (**3h**) also shows complex flower-type structural morphology that is more compact and dense, possibly due to the head−head and tail−tail orientation (Figure 7D). The unique surface morphologies of *alkyl*-ATB derivatives are possibly formed owing to the bipolar self-

https://doi.org/10.1021/acsomega.2c02379
ACS Omega 2022, 7, 27347−27358

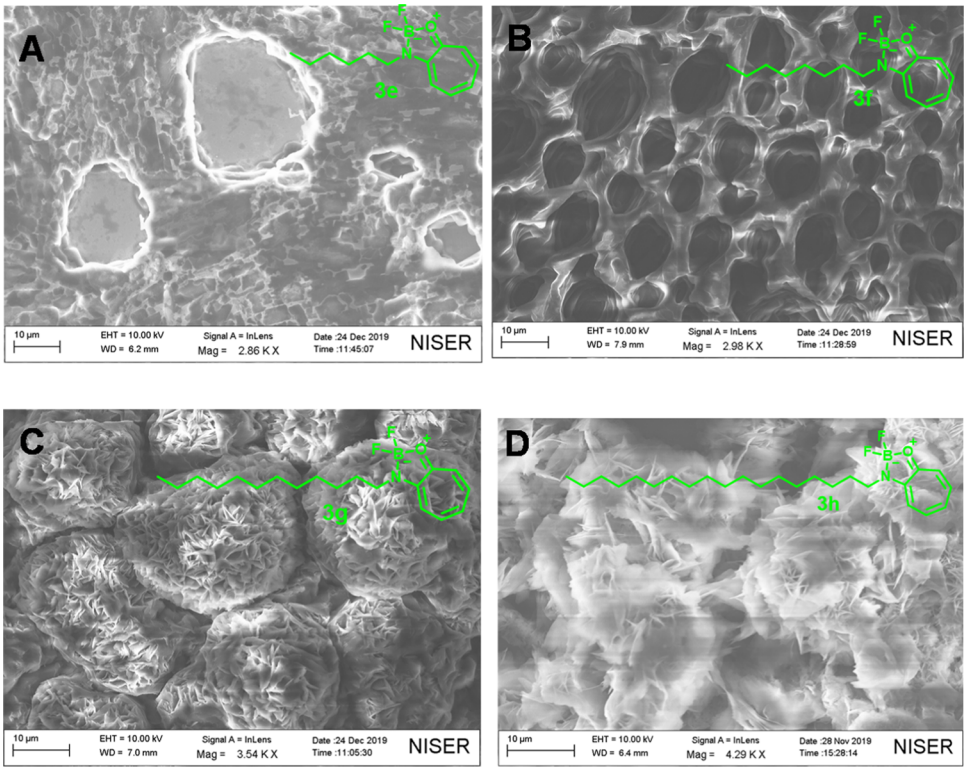

Figure 7. FE-SEM images of *hexyl*-ATB derivative **3b** (A), *octyl*-ATB derivative **3e** (B), *dodecyl*-ATB derivative **3f** (C), and *octadecyl*-ATB derivative **3g** (D) at scale size of 10 μm.

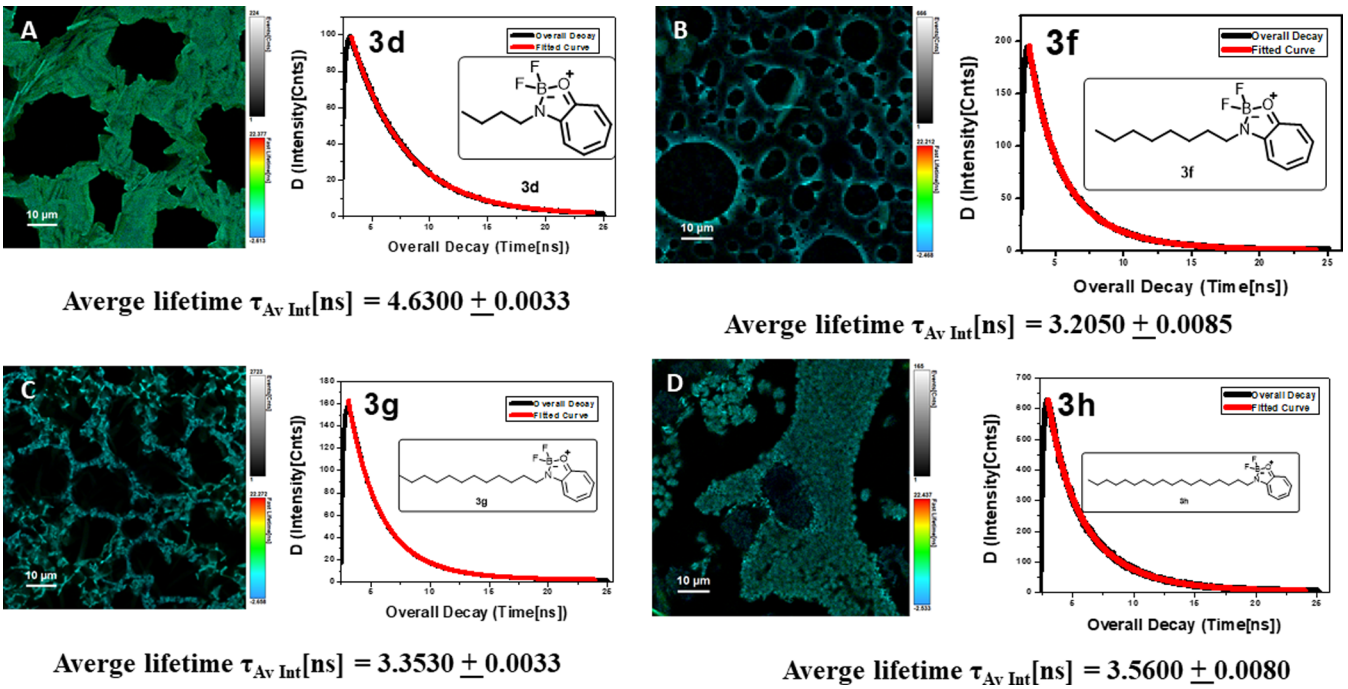

Figure 8. Confocal fluorescence lifetime images and lifetime decay profile of *butyl*-ATB derivative **3d** (A); *octyl*-ATB **3f** (B); *dodecyl*-ATB **3g** (C); and *octadecyl*-ATB **3h** (D).

assembly orientation and strong lipophilic interactions between their long-chain hydrocarbons (tail−tail) along with $\pi-\pi$ interactions between troponyl ring (head−head). Nevertheless, we performed elemental mapping at the unique morphological surface of long-alkyl-chain-containing ATB derivatives (**3g**/**3h**) by SEM-associated energy-dispersive X-ray (EDX) spectrometer. Energy-dispersive X-ray analysis (EDXA) is a technique used for the elemental analysis and concentration determination of nanoparticles by SEM.[32] However, this method has some limitations with regard to accurate dimension and elemental analyses. The EDX data of representative *alkyl*-ATB derivatives (**3g**)/(**3h**) are provided in

https://doi.org/10.1021/acsomega.2c02379
ACS Omega 2022, 7, 27347−27358

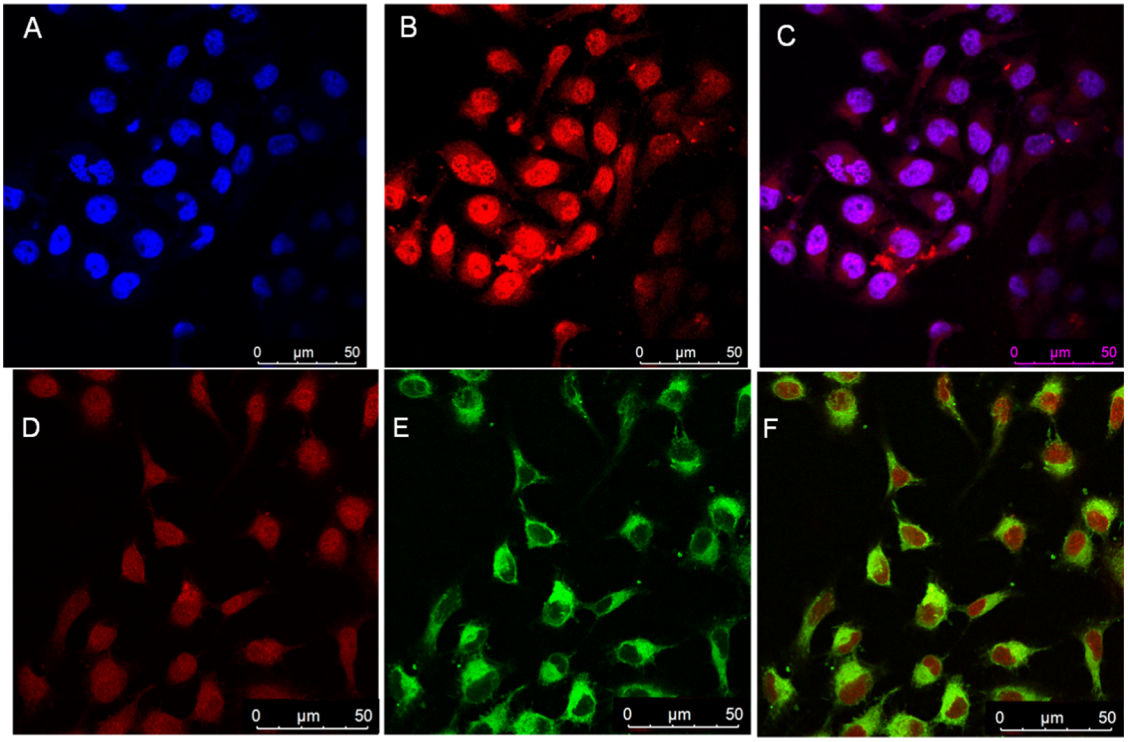

Figure 9. Confocal Image of HeLa cells treated with *octyl*-ATB derivative (**3f**): (A) nuclei were stained with DAPI (blue); (B) cells stained with compound **3f**; (C) merged image of (A) and (B) sections; (D) visualization of compound stained with **3f** (100 μM) in TRITC channel (red); (E) cells stained with commercial BODIPY (BODIPY 493/503; 2 μM) stain (green); and (F) merged image of (A) and (B) sections. All images were taken at 63×, and a scale bar is provided for reference.

the Supporting Information (Figures S60A−S63B). Herein, elemental composition (atom %) of **3g**/**3h** are extracted from their restive EDX spectrum as C (72.53%), N (5.12%), O (5.48%), B (8.41%), and F (8.46%) for **3g** and C (72.46%), N (5.20%), O (5.74%), B (8.15%), and F (8.46%) for **3h**. These analyses strongly support the presence of **3g**/**3h** compounds at their respective surfaces. Hence, ATB derivatives are capable to form self-assembled supramolecular structures owing to the lipid type of noncovalent interactions.

The lipid biomolecules are prone to form liposome and micelle types of self-assembly supramolecular structures. Since *alkyl*-ATB exhibits fluorescence characters in the polar and nonpolar solvent with almost equal quantum efficiency, we attempted to record the fluorescence image of *alkyl*-ATB in the solid state using the confocal microscopic technique, unique for single-molecule sensitivity. Fluorescence lifetime imaging (FLIM) is a technique that resolves and displays the lifetimes of individual fluorophores rather than their emission spectra.[33,34] Fluorophores' lifetime can be influenced by environmental parameters such as pH, ion, oxygen concentration, or molecular bonding. It can be used to distinguish fluorophores. We dissolved fluorescent *alkyl*-ATB derivatives (**3d**/**3f**/**3g**/**3h**) in ethanol and prepared the thin layer of the respective derivative at the glass surface. We recorded their separate fluorescence lifetime images at a scale of 10 μm (Figure 8) while at different scales; their pictures are provided in the Supporting Information (Figures S64−S67). We also extracted lifetime fluorescence decay from respective fluorescence images (Figure 8). The *butyl*-ATB (**4d**) exhibits a solid fluorescence surface with irregular morphology with an average lifetime of 4.6 ns, possibly due to the lipid type of structure (Figure 8A). The *octyl*-ATB (**3f**) shows the formation of a ring type of unique fluorescence surface morphology with an average lifetime of 3.2 ns, possibly due to the lipid type of structural organization (Figure 8B). The dodecyl-ATB (**3g**) exhibits a fluorescence surface with irregular morphologies with an average lifetime of 3.3 ns (Figure 8C). The *octadecyl*-ATB (**3h**) exhibits a fluorescence surface, which is compact with a dense average lifetime of 3.5 ns, possibly due to the strong lipophilic interactions of the long hydrocarbon chain (Figure 8D). We also noted that more minor lipophilic derivatives have a little higher fluorescence lifetime. Their images also support the formation of a self-assembly fluorescent structure with a unique arrangement, possibly owing to the lipophilic noncovalent interactions. For comparison, we recorded FLIM of amino acid derivative of troponyl-BODIPY analogue (alanyl-troponyl difluoroboron). Its FLIM images are provided in the Supporting Information (Figure S68), which exhibit its fluorescence behavior scattered over the surface, unlike the long-chain-hydrocarbon-containing ATB derivatives. The fluorescence lifetime of amino acid derivatives is relatively lower than that of ATB derivatives possibly owing to weak fluorescence behavior and poorly aggregated structure in the solid state. These results strongly support that *alkyl*-ATB derivatives (**3d**/**3f**/**3g**/**3h**) are fluorescent in the solid state with an average lifetime of 3−4 ns, and they have the ability to form a unique type of self-assembly structure.

The MTT assay (*in vitro* toxicology assay) is a colorimetric assay for assessing cell metabolic activity and cell viability.[35,36] We examined the cell viability of alkyl-aminotropones (**2d**−**2h**) and *alkyl*-ATB derivatives (**3a**−**3h**) by dose-dependent MTT assay to the cancerous HeLa cell line and normal human HEK293T cell line (see Figures S69 and S70). Our MTT assay

https://doi.org/10.1021/acsomega.2c02379
ACS Omega 2022, 7, 27347−27358

results strongly support that *alkyl*-ATB derivatives (**3a**−**3h**) are nontoxic to both types of cells. Then, we examined the transfection of *alkyl*-ATB derivatives into HeLa cells *in vitro* conditions. These derivatives were incubated for 18 h before fixing the cells for imaging under a fluorescence microscope. Their fluorescence images are provided in the Supporting Information (Figures S71−S73). We noted that the *octyl*-ATB derivative (**3f**) has efficiently transfected into HeLa cells and localized into the cellular cytoplasm/nucleus. For co-localization studies, we also recorded confocal images of the fixed cells and studied their co-localization with nucleus staining dye (DAPI) and lipid staining dye (BODIPY 493/503). Their confocal images are provided in Figure 9. These images clearly indicate that compound **3f** is localized at the nucleus of cells (Figure 9A−C) and lipid environment (Figure 9D,E). In the literature, Pearson's coefficient (r) is used to quantify the co-localization of two probes by fluorescence microscope.[37] We also extracted Pearson's coefficient (*r*) of compound **3f** with standard probes DAPI and BODIPY (493/503) by superimposing their respective images using co-localization quantifying software (JACoP plugin in Fiji: ImageJ).[38] The Pearson's coefficient value of **3f** with DAPI is ∼0.88, while with BODIPY staining agents, it is ∼0.77. These results strongly support that compound **3f** is localized in the cellular lipid environment and nucleus. Thus long-chain-containing *alkyl*-ATB derivatives are localized at the nucleus of cells, which could be applied to develop fluorescent probes of the cellular nucleus environment.

CONCLUSIONS

We have successfully synthesized lipophilic aminotroponyl difluoroboron complexes and nonbenzenoid BODIPY analogues from Tropolone. We have also shown the structural organization of four crystal complexes in solid states. Their crystal packing diagram shows the formation of supramolecular self-assembly structure with an intermolecular hydrogen bonding between C−H···F. Importantly, these complexes exhibit fluorescence character in the organic solvents (MeOH/ACN) with quantum yield ∼10 to 13% and Stoke'shift 110 nm. Their surface morphologies are demonstrated by the SEM imaging technique, which reveals the role of lipophilic alkyl substituents in the formation of unique self-assembly structures. These complexes also exhibit fluorescence characters in the solid state with a relatively low quantum yield compared to solution. Their self-assembly surface morphologies are also demonstrated by confocal imaging techniques that strongly support supramolecular structure formation with lipophilic alkyl substituents. We have shown their biological relevance by examining cell cytotoxicity and cell transfection in human cells (HEK292). In vitro studies reveal that these analogies are nontoxic to normal human cells. We successfully showed the delivery of *octyl*-aminotroponyl-BODIPY analogue into the HeLa cell line, which becomes fluorescent. Hence, these BODIPY analogues are the potential candidate to design the fluorescence probes of cellular components.

EXPERIMENTAL PROCEDURE

General Information. Unless noted, all required materials and solvents were purchased from commercial suppliers and used without any further purification unless noted. Anhydrous dichloromethane was freshly prepared by distilling over calcium hydride. Reactions were monitored by thin-layer chromatography and visualized by UV and Ninhydrin. Column chromatography was performed in 100−200 mesh silica. Mass spectra were obtained from a Bruker micrOTOF-Q II spectrometer, and the samples were prepared in methanol and injected into a methanol and water mixture. NMR spectra were recorded on a Bruker AV-400 at room temperature (^{1}H: 400 MHz, ^{13}C: 100.6 MHz, ^{11}B: 128 MHz, ^{19}F: 377 MHz). ^{1}H, ^{13}C, ^{11}B, and ^{19}F NMR chemical shifts were recorded in ppm, downfield from tetramethylsilane. Splitting patterns are abbreviated as s, singlet; d, doublet; dd, doublet of doublet; t, triplet; q, quartet; m, multiplet. All boron complex crystal data were collected on a Rigaku Oxford diffractometer at 293 K, respectively. Absorption spectra were obtained using a Jasco V-730 spectrometer. Fluorescence spectra were obtained from a PerkinElmer LS-55 using a xenon lamp. All spectroscopic measurements were carried out with spectroscopic-grade nondegassed solvents and at 20 °C. Relative fluorescence quantum yields were compared with quinine sulfate quantum yield in 0.1 M H_2SO_4 (0.54). The obtained values were substituted in the following equation.

$$\phi_x = \phi_r \times \frac{F_x}{F_r} \times \frac{1 - 10^{-A_r}}{1 - 10^{-A_x}} \times \frac{\eta_x^2}{\eta_x^2}$$

Solid emission of boron complex **3f**, **3g**, and **3h** (excited at 340 and 380 nm) is measured by Edinburgh Instruments FLS 920. HRMS was analyzed with an Agilent Q-TOF 6500.

General Procedure for the Synthesis of *Alkyl*-Aminotropone (2a−2h). All aminotropones were synthesized by following the reported procedure. 2-Tosyloxytropone and amines (1.2 equiv) were dissolved in ethanol; to this, Et3N (3.0 equiv) was added. The reaction mixture was allowed to reflux for 24−36 h. TLC monitored the completion of the reaction. All volatiles were evaporated under reduced pressure after reaction completion. To the crude product, 1.0 N HCl was added and extracted with dichloromethane (thrice), and the combined organic layers were dried over Na_2SO_4 and evaporated under reduced pressure. The obtained crude product was purified by silica gel column chromatography using ethylacetate and hexane mixture as the mobile phase.

*Isobutyl-Aminotropone or 2-(Sec-butylamino)cyclohepta-2,4,6-trienone (**2a**).* The pure product was obtained as a yellowish solid (552 mg, 86%). ^{1}H NMR (400 MHz, $CDCl_3$) δ 7.27−7.12 (m, J = 28.0, 11.7 Hz, 3H), 6.65 (t, J = 9.4 Hz, 1H), 6.56 (d, J = 10.5 Hz, 1H), 3.66−3.60 (m, 1H), 2.00 (s, 1H), 1.75−1.60 (m, 2H), 1.28 (d, J = 6.4 Hz, 3H), 0.98 (t, J = 7.4 Hz, 3H). ^{13}C NMR (101 MHz, $CDCl_3$) δ 176.51, 155.03, 137.16, 136.29, 128.03, 121.77, 108.82, 49.45, 29.10, 19.42, 10.40. HRMS (ESI-TOF) m/z: [M + Na] calc. for $C_{11}H_{15}NO$ 200.1046, found 200.1046.

*Cyclohexyl-Aminotropone or 2-(Cyclohexylamino)-cyclohepta-2,4,6-trienone (**2b**).* The pure product was obtained as a yellowish solid (352 mg, 95%). ^{1}H NMR (400 MHz, $CDCl_3$) δ 7.27−7.12 (m, 3H), 6.67−6.58 (m, 2H), 3.50 (t, J = 4 Hz, 1H), 2.05 (d, J = 12 Hz, 2H), 1.84−1.67 (m, 4H), 1.44−1.31 (m, 4H). ^{13}C NMR (101 MHz, $CDCl_3$) δ 176.53, 163.43, 154.63, 137.15, 136.28, 128.06, 121.78, 108.93, 51.06, 32.07, 25.57, 24.66. HRMS (ESI-TOF) m/z: [M + nH] calc. for $C_{13}H_{17}NO$ 204.1383, found 204.1393.

*Propargyl-Aminotropone or 2-(Prop-2-yn-1-ylamino)-cyclohepta-2,4,6-trienone (**2c**).* The pure product was obtained as a yellowish solid (850 mg, 74%). ^{1}H NMR (400 MHz, $CDCl_3$) δ 7.33−7.27 (m, 2H), 7.21 (t, J = 12 Hz, 1H),

https://doi.org/10.1021/acsomega.2c02379
ACS Omega 2022, 7, 27347−27358

6.75 (t, J = 8 Hz, 1H), 6.62 (d, J = 8 Hz, 1H), 4.14 (dd, J = 5.9, 2.4 Hz, 2H), 2.30 (t, J = 2.4 Hz, 1H), 1.67 (s, 1H). $^{13}C\{H\}$ NMR (101 MHz, $CDCl_3$) δ 177.19, 154.49, 137.49, 136.05, 130.07, 123.40, 109.22, 77.87, 72.51, 32.50. HRMS (ESI-TOF) m/z: [M + nH] calc. for $C_{10}H_9NO$ 160.0757, found 160.0759.

*Butyl-Aminotropone or 2-(Butylamino)cyclohepta-2,4,6-trienone (**2d**).* The pure product was obtained as a yellowish solid (327 mg, 94%). ^1H NMR (400 MHz, $CDCl_3$) δ 7.28−7.21 (m, 3H), 7.14 (d, J = 12 Hz, 1H), 6.66 (t, J = 12 Hz, 1H), 6.54 (d, J = 12 Hz, 1H), 3.33−3.28 (m, 2H), 1.75−1.70 (m, 2H), 1.47 (dd, J = 16, 8 Hz, 2H), 0.98 (t, J = 8 Hz, 3H). $^{13}C\{H\}$ NMR (101 MHz, $CDCl_3$) δ 176.58, 155.71, 137.27, 136.34, 128.28, 121.97, 108.65, 42.59, 30.47, 20.31, 13.75. HRMS (ESI-TOF) m/z: [M + nH] calc. for $C_{11}H_{15}NO$ 178.1226, found 178.1237.

*Hexyl-Aminotropone or 2-(Hexylamino)cyclohepta-2,4,6-trienone (**2e**).* The pure product was obtained as a yellowish solid (337 mg, 90%). ^1H NMR (400 MHz, $CDCl_3$) δ 7.24 (dd, J = 20.3, 10.4 Hz, 3H), 7.14 (d, J = 8 Hz, 1H), 6.66 (t, J = 8 Hz, 1H), 6.52 (d, J = 12 Hz, 1H), 3.29 (dd, J = 12, 6.5 Hz, 2H), 1.77−1.70 (m, 2H), 1.45−1.42 (m, 2H), 1.33 (d, J = 2.9 Hz, 4H), 0.90 (t, J = 5.9 Hz, 3H). $^{13}C\{H\}$ NMR (101 MHz, $CDCl_3$) δ 176.57, 155.68, 137.22, 136.31, 128.27, 121.93, 108.61, 42.89, 31.46, 28.41, 26.81, 22.53, 14.00. HRMS (ESI-TOF) m/z: [M + nH] calc. for $C_{13}H_{19}NO$ 206.1539, found 206.1548.

*Octyl-Aminotropone or 2-(Octylamino)cyclohepta-2,4,6-trienone (**2f**).* The pure product was obtained as a yellowish solid (834 mg, 98%). ^1H NMR (400 MHz, $CDCl_3$) δ 7.09 (s, 1H), 6.97−6.84 (m, 3H), 6.37−6.29 (m, 1H), 6.23−6.18 (m, 1H), 2.98−2.91 (m, 2H), 1.43−1.36 (m, 2H), 1.11−1.00 (m, 10H), 0.63−0.59 (m, 3H). $^{13}C\{H\}$ NMR (101 MHz, $CDCl_3$) δ 176.19, 155.37, 136.77, 136.04, 127.88, 121.52, 108.24, 42.61, 31.57, 29.07, 28.98, 28.21, 26.94, 22.44, 13.89. HRMS (ESI-TOF) m/z: [M + nH] calc. for $C_{16}H_{23}NO$ 234.1852, found 234.1843.

*Dodecyl-Aminotropone or 2-(Dodecylamino)cyclohepta-2,4,6-trienone (**2g**).* The pure product was obtained as a yellowish solid (448 mg, 85%). ^1H NMR (400 MHz, $CDCl_3$) δ 7.28−7.12 (m, 4H), 6.64 (t, J = 8 Hz, 1H), 6.51 (d, J = 12 Hz, 1H), 3.28 (d, J = 8 Hz, 2H), 1.76−1.69 (m, 2H), 1.42−1.26 (m, 20H), 0.87 (t, J = 8 Hz, 3H). $^{13}C\{H\}$ NMR (101 MHz, $CDCl_3$) δ 176.56, 155.67, 137.20, 136.29, 128.26, 121.90, 108.58, 42.89, 31.90, 29.62, 29.61, 29.56, 29.50, 29.33, 29.29, 28.45, 27.14, 22.68, 14.11. HRMS (ESI-TOF) m/z: [M + nH] calc. for $C_{19}H_{31}NO$ 290.2478, found 290.2493.

*Octadecyl-Aminotropone or 2-(Octadecylamino)-cyclohepta-2,4,6-trienone (**2h**).* The pure product was obtained as a yellowish solid (649 mg, 96%). ^1H NMR (400 MHz, $CDCl_3$) δ 7.28−7.20 (m, 3H), 7.14 (d, J = 12 Hz, 1H), 6.66 (t, J = 8 Hz, 1H), 6.53 (d, J = 12 Hz, 1H), 3.32−3.27 (m, 2H), 1.76−1.68 (m, 3H), 1.45−1.42 (m, 2H), 1.40−1.28 (m, 29H), 0.88 (t, J = 6.7 Hz, 3H). $^{13}C\{H\}$ NMR (101 MHz, $CDCl_3$) δ 176.61, 155.70, 137.25, 136.30, 128.31, 121.93, 108.59, 42.92, 31.93, 29.71, 29.67, 29.58, 29.51, 29.37, 29.30, 28.47, 27.16, 22.70, 14.12. HRMS (ESI-TOF) m/z: [M + nH] calc. for $C_{25}H_{43}NO$ 374.3417, found 374.3436.

General Procedure for the Synthesis of *Alkyl*-Amintroponyl Difluoroboron (*Alkyl*-ATB) Complex Boron-Aminotropone (3). Aminotropone (**2a**) (1 equiv) was dissolved in anhydrous dichloromethane, and Et_3N (15 equiv) was added. For further reaction, $BF_3{\cdot}OEt_2$ (15 equiv) was added to the resultant reaction mixture and stirred at room temperature. TLC monitored the completion of the reaction, and water was added to quench unreacted $BF_3{\cdot}OEt_2$ that is extracted with dichloromethane (thrice). The combined organic layer was dried over Na_2SO_4 and concentrated under reduced pressure. The crude product was purified through silica gel column chromatography using 100% DCM as the mobile phase. Boron complex **3a** was obtained in 90% yield. The remaining boron complexes were synthesized by following this general procedure.

*NMR Data of Boron-Aminotropones Isobutyl-ATB or 3-(Sec-butyl)-2,2-difluoro-2,3-dihydrocyclohepta[d][1,3,2]-oxazaborol-1-ium-2-uide (**3a**).* The pure product was obtained as a reddish-brown solid (290 mg, 76%).^1H NMR (400 MHz, $CDCl_3$) δ 7.63−7.58 (m, 1H), 7.46 (t, J = 12 Hz, 1H), 7.25 (t, J = 8 Hz, 1H), 7.15 (d, J = 12 Hz, 1H), 7.06 (t, J = 8 Hz, 1H), 3.83 (s, 1H), 1.98−1.91 (m, 1H), 1.81−1.74 (m, 1H), 1.44 (d, J = 4 Hz, 3H), 0.98 (t, J = 8 Hz, 3H). $^{13}C\{H\}$ NMR (101 MHz, $CDCl_3$) δ 167.33, 159.59, 141.10, 139.42, 127.23, 118.54, 117.92, 53.08, 28.02, 18.16, 11.33. ^{11}B NMR (128 MHz, $CDCl_3$) δ 6.08 (t, J = 20.0 Hz). ^{19}F NMR (377 MHz, $CDCl_3$) δ −130.88 (s), −130.93 (s), −130.99 (s), −131.04 (s), −131.11 (s), −131.16 (s), −131.22 (s), −131.27 (s), −132.59 (dd, J = 39.1, 19.1 Hz), −132.82 (dd, J = 39.1, 19.2 Hz). HRMS (ESI-TOF) m/z: [M + Na] calc. for $C_{11}H_{14}BF_2NO$ 248.1031, found 248.1036.

*Cyclohexyl-ATB or 3-Cyclohexyl-2,2-difluoro-2,3-dihydrocyclohepta[d][1,3,2]oxazaborol-1-ium-2-uide (**3b**).* The pure product was obtained as a reddish-brown solid (180 mg, 77%). ^1H NMR (400 MHz, $CDCl_3$) δ 7.65−7.60 (m, 1H), 7.46 (t, J = 10 Hz, 1H), 7.21 (d, J = 12 Hz, 1H), 7.14 (d, J = 12 Hz, 1H), 7.06 (t, J = 10 Hz, 1H), 3.64 (s, 1H), 2.05−2.02 (m, 2H), 1.91−1.71 (m, 4H), 1.41−1.26 (m, 4H). $^{13}C\{H\}$ NMR (101 MHz, $CDCl_3$) δ 141.20, 139.38, 127.33, 118.51, 117.94, 55.17, 30.58, 25.56, 25.26. ^{11}B NMR (128 MHz, $CDCl_3$) δ 6.05 (t, J = 19.2 Hz). ^{19}F NMR (377 MHz, $CDCl_3$) δ −131.55 (dd, J = 41.4 Hz, 19.2 Hz). HRMS (ESI-TOF) m/z: [M + Na] calc. for $C_{13}H_{16}BF_2NO$ 274.1188, found 274.1193.

*Propargyl-ATB or 2,2-Difluoro-3-(prop-2-yn-1-yl)-2,3-dihydrocyclohepta[d][1,3,2]oxazaborol-1-ium-2-uide (**3c**).* The pure product was obtained as a yellowish solid (800 mg, 72%). ^1H NMR (400 MHz, $CDCl_3$) δ 7.78 (t, J = 10 Hz, 1H), 7.63 (t, J = 12 Hz, 1H), 7.38 (dd, J = 25.0, 10.6 Hz, 2H), 7.27−7.21 (m, 1H), 4.32 (s, 2H), 2.31 (s, 1H). $^{13}C\{H\}$ NMR (101 MHz, $CDCl_3$) δ 168.25, 159.89, 142.05, 140.54, 128.45, 120.59, 118.42, 73.00, 32.14, 29.70. ^{11}B NMR (128 MHz, $CDCl_3$) δ 5.76 (t, J = 17.8 Hz). ^{19}F NMR (377 MHz, $CDCl_3$) δ −139.06 (dd, J = 35.8, 17.6 Hz). HRMS (ESI-TOF) m/z: [M + Na] calc. for $C_{10}H_8BF_2NO$ 230.0561, found 230.0563.

*Butyl-ATB 3-butyl-2,2-difluoro-2,3-dihydrocyclohepta[d]-[1,3,2]oxazaborol-1-ium-2-uide (**3d**).* The pure product was obtained as a reddish-brown solid (250 mg, 78%). ^1H NMR (400 MHz, $CDCl_3$) δ 7.65−7.59 (m, 1H), 7.47 (t, J = 10 Hz, 1H), 7.27−7.23 (m, 1H), 7.11−7.04 (m, 2H), 3.56 (t, J = 6 Hz, 2H), 1.79−1.75 (m, 2H), 1.47−1.41 (m, 2H), 0.98 (t, J = 8 Hz, 3H). $^{13}C\{H\}$ NMR (101 MHz, $CDCl_3$) δ 167.43, 159.89, 141.30, 139.48, 127.27, 118.65, 117.49, 43.44, 29.86, 20.57, 13.76. ^{11}B NMR (128 MHz, $CDCl_3$) δ 5.99 (t, J = 18.8 Hz). ^{19}F NMR (377 MHz, $CDCl_3$) δ −138.28 (dd, J = 37.5, 18.2 Hz). HRMS (ESI-TOF) m/z: [M + Na] calc. for $C_{11}H_{14}BF_2NO$ 248.1031, found 248.1044.

https://doi.org/10.1021/acsomega.2c02379
ACS Omega 2022, 7, 27347−27358

*Hexyl-ATB or 2,2-Difluoro-3-hexyl-2,3-dihydrocyclohepta-[d][1,3,2]oxazaborol-1-ium-2-uide (**3e**).* The pure product was obtained as a reddish-brown solid (310 mg, 83%). ^{1}H NMR (400 MHz, $CDCl_3$) δ 7.66−7.61(m, 1H), 7.47 (t, J = 10 Hz, 1H), 7.23 (d, J = 12 Hz, 1H), 7.12−7.05 (m, 2H), 3.54 (t, J = 6 Hz, 2H), 1.81−1.73 (m, 2H), 1.42−1.31(m, 6H), 0.89 (t, J = 8 Hz, 3H). ^{13}C{H} NMR (101 MHz, $CDCl_3$) δ 167.31, 159.85, 141.40, 139.46, 127.40, 118.65, 117.56, 47.08, 43.66, 31.45, 27.79, 26.98, 22.53, 13.99, 8.71. ^{11}B NMR (128 MHz, $CDCl_3$) δ 5.97 (t, J = 18.7 Hz). ^{19}F NMR (377 MHz, $CDCl_3$) δ −138.17 (dd, J = 37.6, 18.0 Hz). HRMS (ESI-TOF) m/z: [M + Na] calc. for $C_{13}H_{18}BF_2NO$ 276.1344, found 276.1354.

*Octyl-ATB 2,2-Difluoro-3-octyl-2,3-dihydrocyclohepta[d]-[1,3,2]oxazaborol-1-ium-2-uide (**3f**).* The pure product was obtained as a reddish-brown solid (216 mg, 81%). ^{1}H NMR (400 MHz, $CDCl_3$) δ 7.65−7.60 (m, 1H), 7.47 (t, J = 10.2 Hz, 1H), 7.24 (t, J = 11.0 Hz, 1H), 7.11−7.05 (m, 2H), 3.54 (t, J = 7.6 Hz, 2H), 1.81−1.74 (m, 2H), 1.40−1.27 (m, 10H), 0.88 (t, J = 8 Hz, 3H). ^{13}C{H} NMR (101 MHz, $CDCl_3$) δ 167.35, 159.86, 141.35, 139.45, 127.34, 118.62, 117.55, 43.68, 31.77, 29.25, 29.18, 27.84, 27.33, 22.61, 14.08. ^{11}B NMR (128 MHz, $CDCl_3$) δ 5.98 (t, J = 18.5 Hz). ^{19}F NMR (377 MHz, $CDCl_3$) δ −138.20 (dd, J = 36.7, 15.2 Hz). HRMS (ESI-TOF) m/z: [M + Na] calc. for $C_{15}H_{22}BF_2NO$ 304.1657, found 304.1659.

*Dodecyl-ATB or 3-Dodeyl-2,2-difluoro-2,3-dihydrocyclohepta[d][1,3,2]oxazaborol-1-ium-2-uide (**3g**).* The pure product was obtained as a reddish-brown solid (326 mg, 87%). ^{1}H NMR (400 MHz, $CDCl_3$) δ 7.62 (t, J = 10 Hz 1H), 7.48 (t, J = 10 Hz, 1H), 7.28−7.25 (m, 1H), 7.12−7.06 (m, 2H), 3.56 (t, J = 8 Hz, 2H), 1.81−1.77 (m, 2H), 1.42−1.28 (m, 18H), 0.90 (t, J = 6 Hz, 3H). ^{13}C{H} NMR (101 MHz, $CDCl_3$) δ 167.49, 159.86, 141.27, 139.46, 127.24, 118.60, 117.48, 43.70, 31.91, 29.62, 29.57, 29.52, 29.33, 29.30, 27.84, 27.35, 22.68, 14.11. ^{11}B NMR (128 MHz, $CDCl_3$) δ 5.98 (t, J = 18.3 Hz). ^{19}F NMR (377 MHz, $CDCl_3$) δ −138.27 (dd, J = 37.1, 17.0 Hz). HRMS (ESI-TOF) m/z: [M + Na] calc. for $C_{19}H_{30}BF_2NO$ 360.2284, found 360.2296.

*Octadecyl-ATB or 2,2-Difluoro-3-octadecyl-2,3-dihydrocyclohepta[d][1,3,2]oxazaborol-1-ium-2-uide (**3h**).* The pure product was obtained as a white solid (270 mg, 80%).^{1}H NMR (400 MHz, $CDCl_3$) δ 7.61 (t, J = 10 Hz, 1H), 7.47 (t, J = 10 Hz, 1H), 7.26−7.23 (m, 1H), 7.09−7.04 (m, 2H), 3.54 (t, J = 8 Hz, 2H), 1.81−1.74 (m, 2H), 1.61 (s, 1H), 1.40−1.26(m, 30H), 0.88 (t, J = 6.4 Hz, 3H). ^{13}C{H} NMR (101 MHz, $CDCl_3$) δ 167.46, 159.84, 141.24, 139.47, 127.21, 118.62, 117.48, 43.71, 31.93, 29.71, 29.67, 29.64, 29.58, 29.54, 29.37, 29.31, 27.84, 27.36, 22.70, 14.13. ^{11}B NMR (128 MHz, $CDCl_3$) δ 5.98 (t, J = 18.1 Hz). ^{19}F NMR (377 MHz, $CDCl_3$) δ −138.29 (dd, J = 36.8, 16.6 Hz). HRMS (ESI-TOF) m/z: [M + Na] calc. for $C_{25}H_{42}BF_2NO$ 444.3224, found 444.3232.

■ ASSOCIATED CONTENT

Supporting Information

The Supporting Information is available free of charge at https://pubs.acs.org/doi/10.1021/acsomega.2c02379.

NMR and HRMS data of all new compounds, full-range UV−vis and fluorescence spectra of BODIPY derivatives, SEM images of different sizes, and fluorescence microscopy and confocal images (PDF)

3a data (CIF)

3b data (CIF)

3c data (CIF)

3g data (CIF)

■ AUTHOR INFORMATION

Corresponding Author

Nagendra K. Sharma − *School of Chemical Sciences, National Institute of Science Education and Research (NISER) Bhubaneswar, Jatni 752050 Odisha, India; Homi Bhabha National Institute (HBNI), Mumbai 400094, India;* orcid.org/0000-0003-0901-0523; Phone: +91-674-249-4141; Email: nagendra@niser.ac.in

Authors

Bibhuti Bhusana Palai − *School of Chemical Sciences, National Institute of Science Education and Research (NISER) Bhubaneswar, Jatni 752050 Odisha, India; Homi Bhabha National Institute (HBNI), Mumbai 400094, India*

Supriya Kumari − *School of Chemical Sciences, National Institute of Science Education and Research (NISER) Bhubaneswar, Jatni 752050 Odisha, India; School of Biological Sciences, National Institute of Science Education and Research (NISER) Bhubaneswar, Jatni 752050 Odisha, India*

Manjusha Dixit − *School of Biological Sciences, National Institute of Science Education and Research (NISER) Bhubaneswar, Jatni 752050 Odisha, India; Homi Bhabha National Institute (HBNI), Mumbai 400094, India*

Complete contact information is available at: https://pubs.acs.org/10.1021/acsomega.2c02379

Notes

The authors declare no competing financial interest.

■ ACKNOWLEDGMENTS

B.B.P. is grateful to the UGC JRF/SRF research fellowship. The authors thank Rama Chandra Soren for helping with photophysical studies. The authors thank Ayendrila Das for helping in the FLIM-recording of *alkyl*-ATB derivatives, and Department of Biotechnology, Government of India (grant no. BT/PR26143/GET/119112/2017), for financial support.

■ REFERENCES

(1) Zaumseil, J.; Sirringhaus, H. Electron and ambipolar transport in organic field-effect transistors. *Chem. Rev.* **2007**, *107*, 1296−1323.

(2) Bessette, A.; Hanan, G. S. Design, synthesis and photophysical studies of dipyrromethene-based materials: insights into their applications in organic photovoltaic devices. *Chem. Soc. Rev.* **2014**, *43*, 3342−3405.

(3) Kim, H. N.; Guo, Z.; Zhu, W.; Yoon, J.; Tian, H. Recent progress on polymer-based fluorescent and colorimetric chemosensors. *Chem. Soc. Rev.* **2011**, *40*, 79−93.

(4) Ulrich, G.; Ziessel, R.; Harriman, A. The chemistry of fluorescent bodipy dyes: versatility unsurpassed. *Angew. Chem., Int. Ed.* **2008**, *47*, 1184−1201.

(5) Durantini, A. M.; Heredia, D. A.; Durantini, J. E.; Durantini, E. N. BODIPYs to the rescue: Potential applications in photodynamic inactivation. *Eur. J. Med. Chem.* **2018**, *144*, 651−661.

(6) Clarke, R. G.; Hall, M. J. Recent developments in the synthesis of the BODIPY dyes. *Adv. Heterocycl. Chem.* **2019**, *128*, 181−261.

(7) Wang, J.; Li, Y.; Gong, Q.; Wang, H.; Hao, E.; Lo, P.-C.; Jiao, L. *β*-AlkenylBODIPY dyes: Regioselective synthesis via oxidative C−H olefination, photophysical properties, and bioimaging studies. *J. Org. Chem.* **2019**, *84*, 5078−5090.

(8) Golden, J. H.; Facendola, J. W.; Sylvinson MR, D.; Baez, C. Q.; Djurovich, P. I.; Thompson, M. E. Boron dipyridylmethene (DIPYR)

dyes: shedding light on pyridine-based chromophores. *J. Org. Chem.* **2017**, *82*, 7215−7222.
(9) Dorh, N.; Zhu, S.; Dhungana, K. B.; Pati, R.; Luo, F.-T.; Liu, H.; Tiwari, A. BODIPY-based fluorescent probes for sensing protein surface-hydrophobicity. *Sci. Rep.* **2015**, *5*, No. 18337.
(10) Lee, B.; Park, B. G.; Cho, W.; Lee, H. Y.; Olasz, A.; Chen, C. H.; Park, S. B.; Lee, D. BOIMPY: Fluorescent Boron Complexes with Tunable and Environment-Responsive Light-Emitting Properties. *Chem. − Eur. J.* **2016**, *22*, 17321−17328.
(11) Patalag, L. J.; Ho, L. P.; Jones, P. G.; Werz, D. B. Ethylene-bridged oligo-BODIPYs: access to intramolecular J-aggregates and superfluorophores. *J. Am. Chem. Soc.* **2017**, *139*, 15104−15113.
(12) Ray, C.; Díaz-Casado, L.; Avellanal-Zaballa, E.; Bañuelos, J.; Cerdán, L.; García-Moreno, I.; Moreno, F.; Maroto, B. L.; López-Arbeloa, Í.; de la Moya, S. N-BODIPYs Come into Play: Smart Dyes for Photonic Materials. *Chem. − Eur. J.* **2017**, *23*, 9383−9390.
(13) Vu, T. T.; Badre, S.; Dumas-Verdes, C.; Vachon, J.-J.; Julien, C.; Audebert, P.; Senotrusova, E. Y.; Schmidt, E. Y.; Trofimov, B. A.; Pansu, R. B.; et al. New hindered BODIPY derivatives: solution and amorphous state fluorescence properties. *J. Phys. Chem. C* **2009**, *113*, 11844−11855.
(14) Löwik, D. W. P. M.; van Hest, J. C. Peptide based amphiphiles. *Chem. Soc. Rev.* **2004**, *33*, 234−245.
(15) Hungerford, G.; Allison, A.; McLoskey, D.; Kuimova, M. K.; Yahioglu, G.; Suhling, K. Monitoring sol-to-gel transitions via fluorescence lifetime determination using viscosity sensitive fluorescent probes. *J. Phys. Chem. B* **2009**, *113*, 12067−12074.
(16) Arranja, C. T.; Aguiar, A.; Encarnação, T.; Fonseca, S. M.; Justino, L. L.; Castro, R. A.; Benniston, A.; Harriman, A.; Burrows, H. D.; Sobral, A. J. Double-tailed long chain BODIPYs-Synthesis, characterization and preliminary studies on their use as lipid fluorescence probes. *J. Mol. Struct.* **2017**, *1146*, 62−69.
(17) Bentley, R. A fresh look at natural tropolonoids. *Nat. Prod. Rep.* **2008**, *25*, 118−138.
(18) Guo, H.; Roman, D.; Beemelmanns, C. Tropolone natural products. *Nat. Prod. Rep.* **2019**, *36*, 1137−1155.
(19) Liu, N.; Song, W.; Schienebeck, C. M.; Zhang, M.; Tang, W. Synthesis of Naturally Occurring Tropones and Tropolones. *Tetrahedron* **2014**, *70*, 9281−9305.
(20) Hojo, M.; Hasegawa, H.; Yoneda, H. Role of triple ion formation in the acid−base reaction between tropolone and triethylamine in acetonitrile. *J. Chem. Soc., Perkin Trans. 2* **1994**, 1855−1859.
(21) Hojo, M.; Ueda, T.; Inoue, T.; Ike, M.; Kobayashi, M.; Nakai, H. UV−Visible and 1H or 13C NMR Spectroscopic Studies on the Specific Interaction between Lithium Ions and the Anion from Tropolone or 4-Isopropyltropolone (Hinokitiol) and on the Formation of Protonated Tropolones in Acetonitrile or Other Solvents. *J. Phys. Chem. B* **2007**, *111*, 1759−1768.
(22) Breheret, E.; Martin, M. Electronic relaxation of troponoids: tropolone fluorescence. *J. Lumin.* **1978**, *17*, 49−60.
(23) de Sá, G.; Malta, O.; de Mello Donegá, C.; Simas, A.; Longo, R.; Santa-Cruz, P.; da Silva, E., Jr. Spectroscopic properties and design of highly luminescent lanthanide coordination complexes. *Coord. Chem. Rev.* **2000**, *196*, 165−195.
(24) Takagi, K.; Saiki, K.; Mori, K.; Yuki, Y.; Suzuki, M. Synthesis of tropolone-containing conjugated polymers and their optical properties. *Polym. J.* **2007**, *39*, 813.
(25) Balachandra, C.; Sharma, N. K. Novel fluorophores: Syntheses and photophysical studies of boron-aminotroponimines. *Dyes Pigm.* **2017**, *137*, 532−538.
(26) Palai, B. B.; Soren, R.; Sharma, N. K. BODIPY analogues: synthesis and photophysical studies of difluoro boron complexes from 2-aminotropone scaffolds through N, O-chelation. *Org. Biomol. Chem.* **2019**, *17*, 6497−6505.
(27) Sun, F.; Yang, G.; Zhang, Q.; Xue, Z.; Gu, C.; Chen, Z.; Yan, B.; Feng, Y.; Wang, Z.; Meng, S. The self-assembly of monosubstituted BODIPY and HFBI-RGD. *RSC Adv.* **2018**, *8*, 21472−21479.
(28) Lincoln, R.; Greene, L. E.; Zhang, W.; Louisia, S.; Cosa, G. Mitochondria alkylation and cellular trafficking mapped with a lipophilic BODIPY−acrolein fluorogenic probe. *J. Am. Chem. Soc.* **2017**, *139*, 16273−16281.
(29) Vázquez-González, V.; Mayoral, M. J.; Chamorro, R.; Hendrix, M. M.; Voets, I. K.; González-Rodríguez, D. Noncovalent synthesis of self-assembled nanotubes through decoupled hierarchical cooperative processes. *J. Am. Chem. Soc.* **2019**, *141*, 16432−16438.
(30) Walde, P.; Ichikawa, S. Lipid Vesicles and Other Polymolecular Aggregates—From Basic Studies of Polar Lipids to Innovative Applications. *Appl. Sci.* **2021**, *11*, 10345.
(31) Kundu, N.; Banik, D.; Sarkar, N. Self-assembly of amphiphiles into vesicles and fibrils: investigation of structure and dynamics using spectroscopy and microscopy techniques. *Langmuir* **2018**, *34*, 11637−11654.
(32) Zadora, G.; Brożek-Mucha, Z. SEM−EDX—a useful tool for forensic examinations. *Mater. Chem. Phys.* **2003**, *81*, 345−348.
(33) Whelan, D. R.; Bell, T. D. Super-resolution single-molecule localization microscopy: tricks of the trade. *J. Phys. Chem. Lett.* **2015**, *6*, 374−382.
(34) Thiele, J. C.; Helmerich, D. A.; Oleksiievets, N.; Tsukanov, R.; Butkevich, E.; Sauer, M.; Nevskyi, O.; Enderlein, J. Confocal fluorescence-lifetime single-molecule localization microscopy. *ACS Nano* **2020**, *14*, 14190−14200.
(35) Plumb, J. A. Cell Sensitivity Assays: The MTT Assay. In *Cancer Cell Culture*, Springer, 2004; pp 165−169.
(36) Yang, Y.; Guo, Q.; Chen, H.; Zhou, Z.; Guo, Z.; Shen, Z. Thienopyrrole-expanded BODIPY as a potential NIR photosensitizer for photodynamic therapy. *Chem. Commun.* **2013**, *49*, 3940−3942.
(37) Bolte, S.; Cordelières, F. P. A guided tour into subcellular colocalization analysis in light microscopy. *J. Microsc.* **2006**, *224*, 213−232.
(38) Dunn, K. W.; Kamocka, M. M.; McDonald, J. H. A practical guide to evaluating colocalization in biological microscopy. *Am. J. Physiol. Cell Physiol.* **2011**, *300*, C723−C742.

https://doi.org/10.1021/acsomega.2c02379
ACS Omega 2022, 7, 27347−27358